A Calculation Method of Dynamic Thrust of SLIM for Mid-Low Speed Maglev

Zhihua Zhang
Graduate School of Chinese Academy of Sciences, Beijing 100039, China
zzhua@mail.iee.ac.cn,

Liming Shi
Key Laboratory of Power Electronics and Electric Drive
Institute of Electrical Engineering, Chinese Academy of Sciences, Beijing, 100190, China
National Maglev Transportation Engineering R&D Center, 201204, China
limings @mail.iee.ac.cn,

ABSTRACT: A dynamic thrust calculation method is proposed on the basis of gap flux density and motor speed. In this method, the steady and dynamic end effect of SLIM are considered with less coupling parameters. Then the aberrance extent of magnetic flux density at different slip frequency and the influence to dynamic thrust of SLIM is analyzed. Using this method, a SLIM can be optimized to increase running speed with same power capacity. The simplicity and accuracy of the method are verified by FEM and experimental results.

1 INTRODUCTION

Although single-sided linear induction motor (SLIM) has many advantages in mid-low speed maglev vehicle drive, how to meet the needs of providing large thrust force and reaching required speed under same motor size with same power voltage is a practical issue. To obtain large acceleration, constant current is generally controlled, but thrust force decrease with the speed increasing. Meanwhile, the general calculation method of equivalent circuit [1]-[5] considers only the influence of SLIM dynamic end effect to excitation of the motor. The thrust force is calculated by electromagnetic field analysis, in which the traditional induction motor equivalent circuit is revised by longitudinal and transverse end effect factors. These parameters of mathematical model are much difficult for SLIM since the mutual inductance and flux are not equal in three-phase windings.

It is known that *x* axis component in the secondary current will increase with secondary resistivity in real reaction plate. This is usually compensated by complicated Russel-Norsworthy factor.

In this paper, the dynamic process of SLIM is analyzed based on dynamic operating characteristics of SLIM with the longitudinal end effect in the motor dynamic process. The dynamic density distribution of gap flux at different speed is obtained, then a novel method to calculate SLIM steady and dynamic thrust is proposed. By adjusting a inflection point parameter, characteristics of thrust force can be optimized.

2 SLIM STEADY MAGNETIC FIELD ANALYSIS

Gap flux in steady is generally affected by the static end effect. Besides travelling magnetic field in gap, static end effect generates pulsating flux which make the gap flux density fluctuate along the *y* axis direction. The average of synthetic flux density is constant with time. Fig. 1 shows the analytical model of the SLIM. Here, the conductivity of primary core and secondary steel plate is considered as zero. Flux density only has *y* component and line current density only has *z* component.

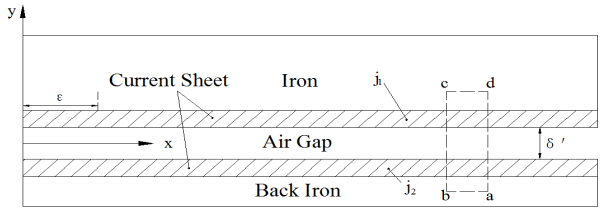

Figure 1. Analytical model of the SLIM

The following equations are established along the rectangular path (abcd).

$$\frac{\delta'}{\mu_0}\frac{\partial B_y}{\partial x} = j_1 + j_2 . \tag{1}$$

$$\frac{\partial B_y}{\partial t} + V_x \frac{\partial B_y}{\partial x} = \frac{\partial E_z}{\partial x} . \tag{2}$$

where δ' is effective electromagnetic air gap, μ_0 is air permeability, j_1, j_2 are primary and secondary line current density respectively, E_Z is secondary induced electric field strength and v_x is secondary velocity. The primary and secondary line current density is

$$j_1 = \frac{mWk_w I_1}{P\tau} . \tag{3}$$

$$j_2 = E_z \sigma_s \tag{4}$$

where m is motor phases, W is winding turns per phase, k_w for winding factor, P is the number of pole pairs, τ is pole pitch, σ_S is surface conductivity of the secondary conductive plate. Gap flux density equation is obtained from the above four equations.

$$\frac{\delta'}{\mu_0}\frac{\partial^2 B_y}{\partial x^2} - v_x\sigma_s\frac{\partial B_y}{\partial x} - \sigma_s\frac{\partial B_y}{\partial t} = \frac{\partial j_1}{\partial x} . \tag{5}$$

Considering the characteristics of the two half-filled slot in SLIM, the primary line current density decreased into one half in range of ε as included in (5). The gap flux density is

$$B_{y1} = B_{y3} = \frac{0.5\mathrm{j}\pi J_1}{\delta'\pi^2/\mu_0\tau + \mathrm{j}\tau s\omega\sigma_s} e^{\mathrm{j}(\omega t - kx)} \quad . \tag{6}$$
$$0 < x \le \varepsilon \cup (2p\tau - \varepsilon) < x \le 2p\tau$$

$$B_{y2} = \frac{\mathrm{j}\pi J_1}{\delta'\pi^2/\mu_0\tau + \mathrm{j}\tau s\omega\sigma_s} e^{\mathrm{j}(\omega t - kx)} \quad . \tag{7}$$
$$\varepsilon < x \le (2p\tau - \varepsilon)$$

where, ε is the length of half filled slot area, J_1 for the amplitude of traveling wave current layer, ω for angular frequency. When slip s = 1, the steady-static flux density in gap distribution can be obtained.

3 DYNAMIC PROCESS ANALYSIS OF SLIM

During acceleration, SLIM used on maglev train is with constant AC current and flux density so that the output thrust is basically constant by using variable voltage variable frequency (VVVF) control. As the speed increases, the inverter output voltage reaches its limit. Then the inverter uses constant power control and motor thrust decreases.

During the moving of SLIM, the motor induces different eddy current at both ends of the secondary plate, which results in the flux density distortion as shown in Fig.2. Gap flux density in the entrance of the movement direction increases from zero to a stable value, meanwhile that decreases rapidly in the exit. Here, we only analyze the effects of the flux density distortion to the thrust in the entrance.

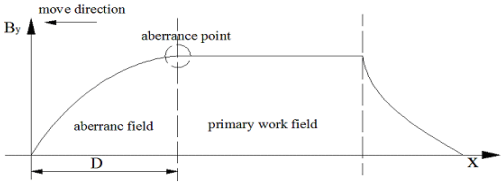

Figure 2. Dynamic air-gap flux density distribution of SLIM

In the entrance area of SLIM， the time constant T_r of secondary is

$$T_r = L_r / R_r . \tag{8}$$

where, L_r is the secondary inductance, R_r the secondary resistance, dynamic gap flux density of the motor in aberrance field can be written as (9).

$$B_y = (1 - e^{-t/T_r})\, B_y . \tag{9}$$

It is the first-order zero state response of gap flux density. The flux density reaches a stable value after the time of 3 T_r to 5 T_r. Setting a inflection point parameter at the point where flux density is close to the stable value, the length can be got by

$$\mathrm{D} = KT_r v \qquad 3 \le K \le 5 . \tag{10}$$

K is solution accuracy factor, v is velocity of linear induction motor.

From (10) we know that the higher the velocity of motor is the greater influence is due to the dynamic end effect, and the position of stable inflection point move back. This results in distortion increase of gap flux, thrust decrease and poor motor performance, then operation may become unstable or speed be limited.

In the aberration range of flux density, (9) can be translated into another equation which is expressed by distance and the speed of motor.

$$B_y(x) = (1 - e^{-x/(vT_r)})B_y \qquad 0 \le x \le \mathrm{D} . \tag{11}$$

4 STEADY AND DYNAMIC THRUST CALCULATION

According to the relationship among thrust and primary line current and gap flux density. The steady thrust of SLIM is derived as shown in (12)

$$F = L(\int_0^{\varepsilon} 0.5 j_1 \left|B_{y1}\right| dx + \int_{\varepsilon}^{2p\tau-\varepsilon} j_1 \left|B_{y2}\right| dx + \int_{2p\tau-\varepsilon}^{2p\tau} 0.5 j_1 \left|B_{y3}\right| dx) \quad (12)$$

where, L is the width of primary core.

Fig.3 shows the dynamic flux density distribution with different speed by using the dynamic gap flux density (11) as correction curve in steady gap flux density distribution. The dynamic end effect is quantized in steady thrust calculation.

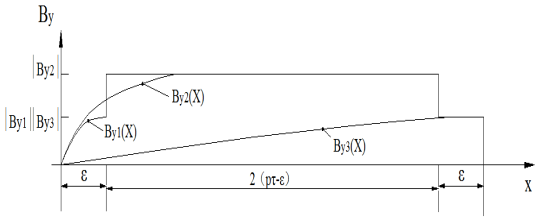

Fig 3. Compensated flux density distribution with different speed

When v=v_1, dynamic thrust is

$$F' = L(\int_0^{D} 0.5 J_1 \left|B_{y1}(X)\right| dx + F). \quad (13)$$

when v=v_2, dynamic thrust is

$$F' = L(\int_0^{D} 0.5 J_1 \left|B_{y2}(X)\right| dx + F). \quad (14)$$

when v=v_3, dynamic thrust is

$$F' = L(\int_0^{D} 0.5 J_1 \left|B_{y3}(X)\right| dx + F). \quad (15)$$

where v_1<v_2<v_3, $By1(x)$, $By2(x)$, $By3(x)$ are dynamic gap flux density with aberrance at different speed respectively and F is thrust with steady gap flux density.

5 COMPARISION AND ANALYSIS

Generally, the current of the SLIM is controlled constant at low speed. The finite element model of a SLIM (190KW) is established. Its thrust is simulated in time-harmonic field. The analysis and FEM flux density RMS value are shown in Fig.4.

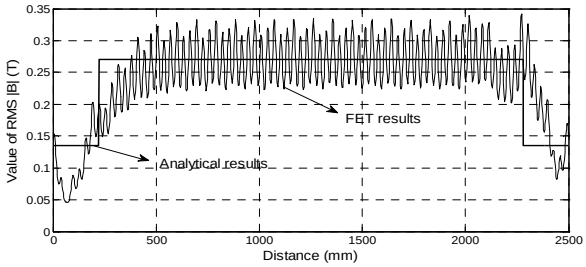

Fig. 4 The FEM and analytical results of B

From the results it is known that the flux density at the range of one-half slot of motor is nearly half of that in middle of the motor, which is consistent with the previous analysis. Steady flux density is the function of gap reluctance between tooth-slot. As two curves is equal, the accuracy of steady thrust calculation is satisfied. Besides, the secondary surface conductivity coefficient should also be compensated when calculating steady gap flux density based on transverse end effect of SLIM.

The secondary time constant Tr is important to solve dynamic thrust of SLIM comparing to the rotary motor Tr since the dynamic end effect reduce the excitation inductance of SLIM. In order to get the accuracy distribution of dynamic gap flux density and the length of inflection point D, it is needed to identify Tr on-line by MRAS as showed in Fig.5.

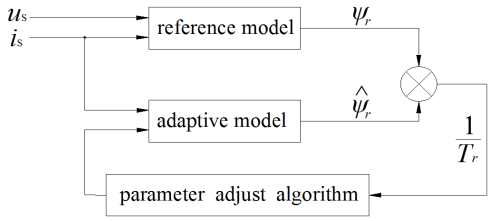

Fig. 5 The principal of Tr by MRAS

With the value of Tr at different speed, dynamic flux density curve can be fitted in different SLIM slip frequency based on the steady-state flux density calculation. Fig. 6 and Fig. 7 show the actual operation characteristics of two traction motors and the calculation results of dynamic thrust.

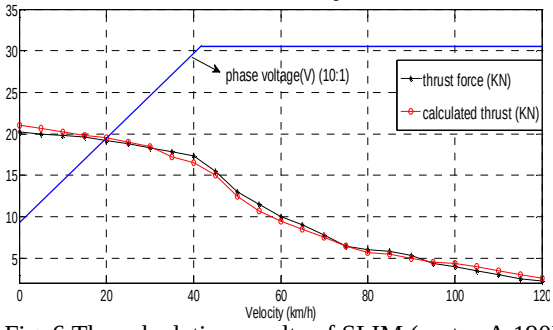

Fig. 6 The calculation results of SLIM (motor A 190KW)

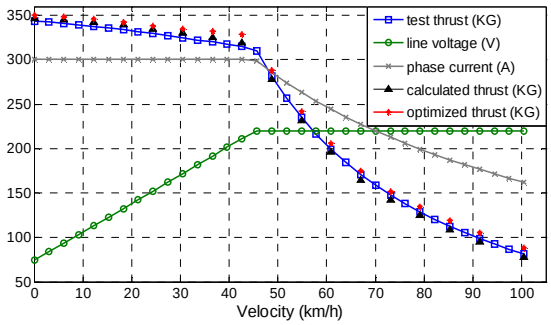

Fig. 7 The calculation results of SLIM (motor B 130KVA)

In Fig.6, at low speed, motor A is controlled with constant thrust till the speed of 40km/h, but the thrust drop about 16% due to the dynamic end effect with the motor speed increase. Calculation thrust is little higher than test because Tr identified by MRAS is not very accurate at that speed. At high speed, the secondary time constant changes greatly because of decreasing magnetizing inductance. As the dynamic end effect of SLIM becomes more serious, Tr obtained from MRAS revises the distribution of flux density timely and calculation results agree well with the test at high speed.

Comparison on motor A, thrust of motor B drop about 10% in the same stage of constant current control. This indicates the aberrance extent of dynamic gap flux density of motor A more serious than that of motor B. Therefore, it is one of optimizing approach of Tr by decreasing the secondary leakage inductance and increasing appropriately secondary resistance. Through optimizing the secondary of motor B, the decrease trend of thrust is improved, it is about 6% as shown in Fig.7.

Besides, it is possible to enable SLIM reach higher speed without changing power capacity by increasing the number of motor poles and minimizing the length of inflection point D.

6 CONCLUSION

A dynamic thrust calculation method for the SLIM in low-speed maglev based on the field analysis is proposed in this paper. It deals with few coupling parameters considering the static and dynamic end effects. The running performance of SLIM can be valuated to help motor design and optimization to reduce distortion of thrust. SLIM's operation speed can be increased with power capacity by selecting reasonable secondary parameters. Comparison with experiments shows that this method is easy and practical.

7 REFERENCES

Dae-Kyong, K. and K. Byung-Il, A Novel Equivalent Circuit Model of Linear Induction Motor Based on Finite Element Analysis and Its Coupling With External Circuits. Magnetics, IEEE Transactions on, 2006. 42(10): p. 3407-3409.

Duncan, J., Linear induction motor-equivalent-circuit model. Electric Power Applications, IEE Proceedings B, 1983. 130(1): p. 51-57.

Da Silva, E.F., et al. Dynamic model for linear induction motors. in Industrial Technology, 2003 IEEE International Conference on. 2003.

Du, Y. and N. Jin. Research on characteristics of single-sided linear induction motors for urban transit. in Electrical Machines and Systems, 2009. ICEMS 2009. International Conference on. 2009.

Nabiyev, F.M. Mathematical modelling of electromagnetic forces in Linear Induction Motors. in Electrical Machines, 2008. ICEM 2008. 18th International Conference on. 2008.

Nasar, S.A. and L. Del Cid, Jr., Propulsion and levitation forces in a single-sided linear induction motor for high-speed ground transportation. Proceedings of the IEEE, 1973. 61(5): p. 638-644.

Idir, K., G.E. Dawson, and A.R. Eastham, Modeling and performance of linear induction motor with saturable primary. Industry Applications, IEEE Transactions on, 1993. 29(6): p. 1123-1128.

Pai, R., S. Nasar, and I. Boldea, A hybrid method of analysis of low-speed linear induction motors. Magnetics, IEEE Transactions on, 1987. 23(6): p. 3908-3915.

Gieras, J., G. Dawson, and A. Eastham, Performance calculation for single-sided linear induction motors with a double-layer reaction rail under constant current excitation. Magnetics, IEEE Transactions on, 1986. 22(1): p. 54-62.